Article

Current Biology

Coinfecting phages impede each other's entry into the cell

Graphical abstract

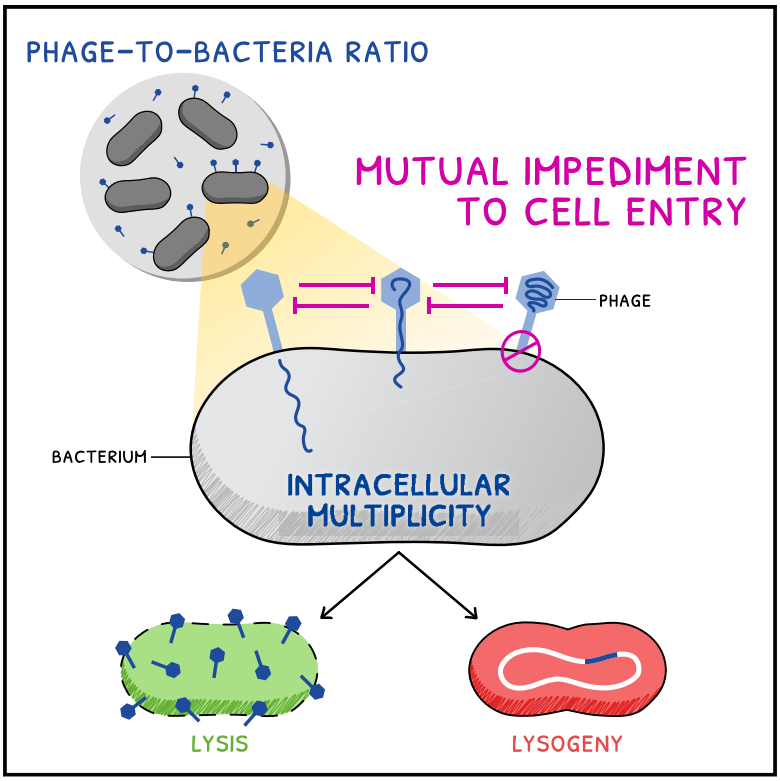

Authors

Thu Vu Phuc Nguyen, Yuchen Wu, Tianyou Yao, Jimmy T. Trinh, Lanying Zeng, Yann R. Chemla, Ido Golding

Correspondence

igolding@illinois.edu

In brief

Nguyen et al. find that when multiple lambda phages infect the same *E. coli* cell, they slow or even prevent each other from entering the cell. Similar behavior is observed in other phages. The impeded entry at high multiplicities, caused by phage-induced perturbation to the host cell, impacts the choice between viral reproduction and dormancy.

Highlights

- Adsorption and genome entry of individual phages were followed in real time
- The efficiency of phage entry decreases at higher multiplicity of infection (MOI)
- Phage entry is impeded at high MOI by adsorption-induced perturbation to the cell
- MOI-dependent phage entry impacts the choice between lysis and lysogeny

Nguyen et al., 2024, Current Biology *34*, 1–13
July 8, 2024
https://doi.org/10.1016/j.cub.2024.05.032

CellPress

Please cite this article in press as: Nguyen et al., Coinfecting phages impede each other's entry into the cell, Current Biology (2024), https://doi.org/10.1016/j.cub.2024.05.032

Current Biology

CellPress

Article

Coinfecting phages impede each other's entry into the cell

Thu Vu Phuc Nguyen,[1,2,7] Yuchen Wu,[3] Tianyou Yao,[1] Jimmy T. Trinh,[4,5] Lanying Zeng,[4,5] Yann R. Chemla,[1,3] and Ido Golding[1,2,6,8,*]

[1]Department of Physics, University of Illinois Urbana-Champaign, Urbana, IL 61801, USA
[2]Verna and Marrs McLean Department of Biochemistry and Molecular Biology, Baylor College of Medicine, Houston, TX 77030, USA
[3]Center for Biophysics and Quantitative Biology, University of Illinois Urbana-Champaign, Urbana, IL 61801, USA
[4]Department of Biochemistry and Biophysics, Texas A&M University, College Station, TX 77843, USA
[5]Center for Phage Technology, Texas A&M University, College Station, TX 77843, USA
[6]Department of Microbiology, University of Illinois Urbana-Champaign, Urbana, IL 61801, USA
[7]Present address: Department of Molecular Biology, Princeton University, Princeton, NJ 08544, USA
[8]Lead contact
*Correspondence: igolding@illinois.edu
https://doi.org/10.1016/j.cub.2024.05.032

SUMMARY

The developmental choice made by temperate phages, between cell death (lysis) and viral dormancy (lysogeny), is influenced by the relative abundance of viruses and hosts in the environment. The paradigm for this abundance-driven decision is phage lambda of *E. coli*, whose propensity to lysogenize increases with the number of viruses coinfecting the same bacterium. It is believed that lambda uses this number to infer whether phages or bacteria outnumber each other. However, this interpretation is premised on an accurate mapping between the extracellular phage-to-bacteria ratio and the intracellular multiplicity of infection (MOI). Here, we show this premise to be faulty. By simultaneously labeling phage capsids and genomes, we find that, while the number of phages landing on each cell reliably samples the population ratio, the number of phages entering the cell does not. Single-cell infections, performed in a microfluidic device and interpreted using a stochastic model, reveal that the probability and rate of phage entry decrease with the number of adsorbed phages. This decrease reflects an MOI-dependent perturbation to host physiology caused by phage attachment, as evidenced by compromised membrane integrity and loss of membrane potential. The dependence of entry dynamics on the surrounding medium results in a strong impact on the infection outcome, while the protracted entry of coinfecting phages increases the heterogeneity in infection outcome at a given MOI. Our findings in lambda, and similar results we obtained for phages T5 and P1, demonstrate the previously unappreciated role played by entry dynamics in determining the outcome of bacteriophage infection.

INTRODUCTION

Bacteriophage lambda serves as a paradigm for the decision made by temperate phages between rampant replication, resulting in the release of viral progeny and cell death (lysis) and dormancy in a prophage state (lysogeny), which allows the host bacterium to live and reproduce.[1,2] The best-characterized factor affecting this choice is the number of lambda phages coinfecting the cell (multiplicity of infection [MOI]).[3,4] Infection by a single phage typically results in lysis, whereas a higher MOI results in lysogeny.[5,6] The effect of MOI is mediated by a phage-encoded circuit that chooses the transcriptional program to be executed based on the number of lambda genomes that entered the cell.[7,8] In terms of its utility, viral self-counting is believed to serve as a way of inferring the abundance of available hosts in the environment.[3,9] Specifically, simultaneous infection by multiple phages (i.e., MOI > 1) implies that phages outnumber bacteria, thus the release of new progeny via lysis will be futile, and lysogeny should be chosen. This interpretation is consistent with other examples where the relative abundance of phages and bacteria impacts infection outcome.[10] However, it is premised on an accurate mapping between the environmental phage-to-bacteria ratio and the intracellular MOI, a mapping that has not been directly tested. This accurate mapping is further called into doubt by the fact that, at the single-cell level, the relation between MOI and infection outcome is highly probabilistic rather than threshold-like.[6,11] Thus, the relationship between the population ratio and the number of internalized phage genomes merits careful examination.

Another motivation to closely inspect phage entry is that our understanding of the process remains fragmentary, even for a system as extensively studied as lambda.[2] For one, there is no consensus regarding the nature of physical forces driving translocation of the encapsidated DNA into the cell.[12] Several competing hypotheses exist, including DNA self-repulsion followed by diffusion,[13] and hydrodynamic drag due to water drainage through the capsid,[14] but the available data are insufficient to determine their veracity. Also unclear is the exact route

Please cite this article in press as: Nguyen et al., Coinfecting phages impede each other's entry into the cell, Current Biology (2024), https://doi.org/10.1016/j.cub.2024.05.032

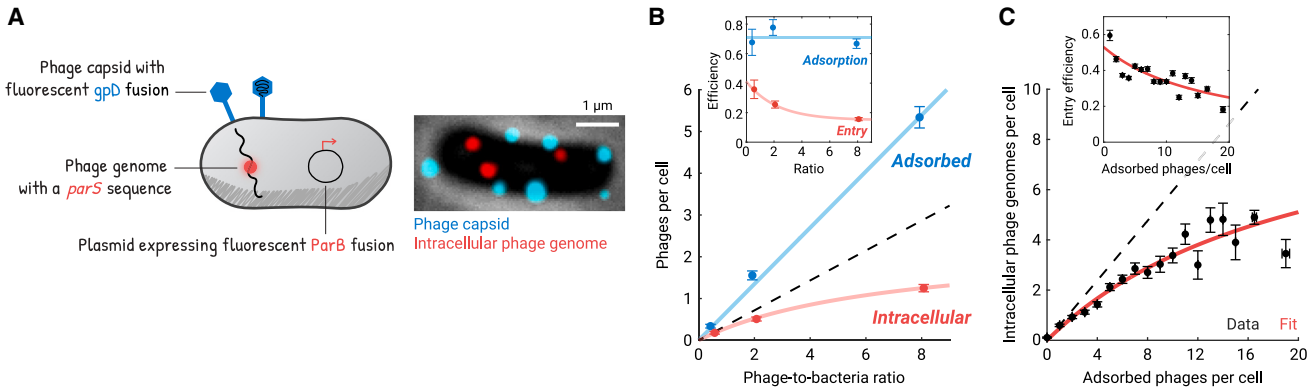

Figure 1. The intracellular viral copy number is not proportional to the extracellular phage-to-bacteria ratio

(A) Phage capsids and intracellular phage genomes were fluorescently labeled. Left: schematic of the labeling system. Right: an *E. coli* cell adsorbed by seven lambda phages (cyan spots), three of which have ejected their genomes (red spots). The infection mixture was imaged 5 min after triggering genome ejection. The image shown is a maximum projection of multiple focal planes, spanning the height of the cell.

(B) The fraction of phages whose genomes entered the cell decreases at higher phage-to-bacteria ratio. Phages and bacteria were mixed at different ratios. Markers, mean ± SE for the average numbers of adsorbed and intracellular phages (n = 201, 204, and 221 cells for samples with mixing ratios of 0.5, 2, and 8, respectively). Cyan line, linear fit. Red curve, fit to a Michaelis-Menten function, serving as a guide to the eye. Dashed line, linear scaling extrapolated from the sample with the phage-to-bacteria ratio of 0.5. Inset: the efficiencies of phage adsorption and entry (defined as the average numbers of adsorbed and intracellular phages per cell, respectively, divided by the phage-to-bacteria ratio).

(C) The number of intracellular phage genomes scales sublinearly with the number of phages adsorbed to the cell. Black markers, mean ± SE (n = 1,437 cells, pooled from 7 independent experiments); cells at higher MOI were binned together to allow for at least 10 cells per bin. Red curve, fit to a Michaelis-Menten function, serving as a guide to the eye. Dashed line, linear scaling extrapolated from cells with one adsorbed phage. Inset: the efficiency of phage entry as a function of the number of adsorbed phages. The red curve was calculated using the same fit as in the main panel.

See also Figure S1.

the phage genome takes to enter the cell: the maltoporin LamB (lambda receptor) is involved in the initial reversible binding to the host surface,[15] the eventual irreversible docking at the site where DNA will cross the cell membrane,[16] and in triggering DNA entry.[17] It is unlikely, however, that phage DNA moves *through* the LamB porin.[18,19] Instead, it is suggested that the phage's tape measure protein (gpH) breaches the outer membrane and then acts as a conduit for DNA translocation through the bacterial periplasm.[19–22] Similarly elusive is how lambda DNA crosses *E. coli*'s inner membrane. Whereas penetration generally requires the inner-membrane mannose phosphotransferase system (PtsM or Man-PTS),[23,24] phages with extended genomes and those harboring certain tail mutations can overcome this requirement.[21,25] Thus, how lambda DNA and PtsM interact during phage entry also remains an open question. Critically, our picture of phage entry is largely inferred from studies of isolated components *in vitro* and from bulk studies where single-cell kinetics remains hidden.[12] There is thus considerable benefit to examining the entry process in its true context of infection, at the resolution of individual phages and cells.

RESULTS

The intracellular viral copy number is not proportional to the extracellular phage-to-bacteria ratio

To examine infection at the single-cell level, we utilized phages (λ *cI857 Pam80 stf*::P1*parS-kan*^{R})[8] whose capsid was decorated with gpD-mTurquoise2 or gpD-EYFP.[26] Following infection (of host MG1655), the intracellular phage genome is detected via binding of mCherry-ParB or CFP-ParB to an engineered *parS* sequence[27,28] (Figure 1A; STAR Methods). The infecting phage is unable to replicate on wild-type host, preventing intracellular genome number from increasing after entry.[8] The labeling scheme enables reliable counting of both extracellular capsids and intracellular phage genomes (Figure S1).

We first asked how the numbers of phages adsorbed (irreversibly attached[29,30]) to the cell and of phages that have entered the cell (intracellular genomes) changed as we infected cells with varying phage concentrations. Cells grown in LB (supplemented with maltose and $MgSO_4$) were concentrated, mixed with phages, and incubated at 4°C for 30 min to allow adsorption; then, to trigger genome ejection, the infection mixture was shifted to 35°C[6,8,29] (STAR Methods). Imaging the infected samples at 5 min after triggering, we found that, over an ~10-fold change in phage concentration, the average number of adsorbed phages per cell followed the phage-to-bacteria ratio (Figure 1B), with the adsorption efficiency remaining constant at 0.71 ± 0.04 (mean ± SE of three samples, n = 201, 204, and 221 cells), consistent with reported values[31–33] (Figure S1). By contrast, the efficiency of phage entry decreased approximately 2-fold (from 0.36 ± 0.06 to 0.16 ± 0.01; Figure 1B). Consequently, the average number of intracellular phage genomes per cell did not reflect the bulk ratio of phages to bacteria.

We next utilized the natural variability in the number of phages adsorbed to each cell[6,8] to probe the relation between the adsorbed and intracellular phage numbers at the single-cell level. We found that as the number of adsorbed phages per cell increased, the efficiency of phage entry decreased: from approximately 60% in cells adsorbed by a single phage (consistent with previous reports[29,33]; Figure S1) to approximately 30% in cells adsorbed by 10 phages (Figure 1C; n = 1,437 cells, pooled from 7 independent experiments). As a result, the number

Please cite this article in press as: Nguyen et al., Coinfecting phages impede each other's entry into the cell, Current Biology (2024), https://doi.org/10.1016/j.cub.2024.05.032

CellPress

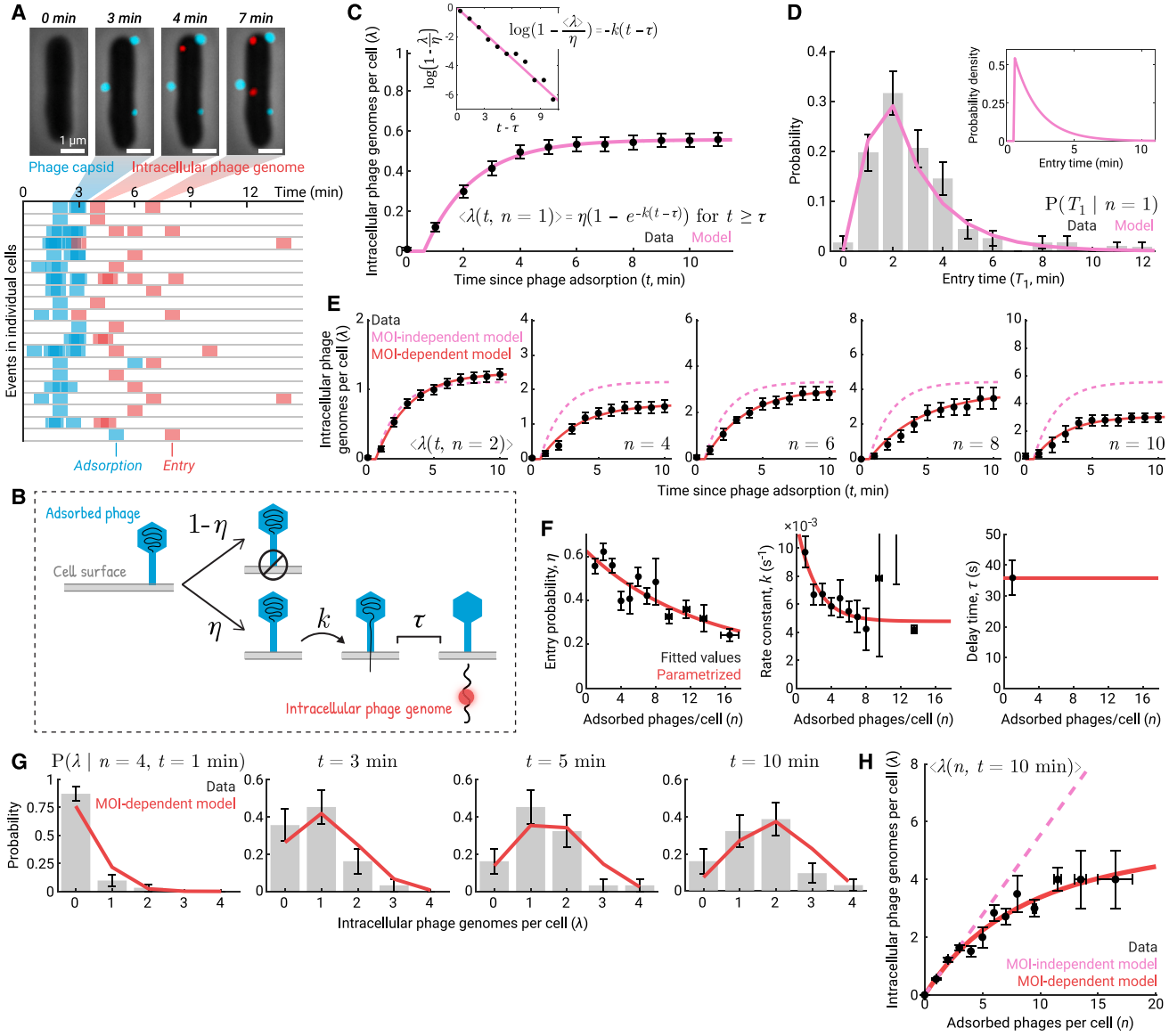

Figure 2. Time-lapse measurements indicate an MOI-dependent decrease in the probability and rate of phage entries

(A) Adsorption and entry of individual phages were followed in a microfluidic device. Top: an infected cell tracked over time. Bottom: for each cell, the times of adsorption and entry events were recorded. Data for 20 cells are shown. For all cells in this experiment, see Figure S2.

(B) Schematic of the stochastic model for phage entry kinetics; see text for details.

(C) The theoretical model captures the time-dependent average number of intracellular phages in cells adsorbed by one phage. Black markers, mean ± SE (n = 208 cells, pooled from 7 independent experiments). Pink curve, fit to the model. Inset: linearized data and model.

(D) The model successfully predicts the distribution of entry times in cells adsorbed by one phage. Gray bars, histogram of the data, with error bars indicating SE. Pink curve, the probability distribution predicted by the model, binned by the imaging inter-frame interval. Inset: the theoretical probability distribution before binning.

(E) A dependence of the entry parameters on the number of adsorbed phages is required to capture the experimental data. Dashed curves in pink, predictions by a model in which η and k in cells adsorbed by multiple phages are equal to those in cells adsorbed by a single phage. Solid curves in red, predictions by a model in which η and k are allowed to vary with the number of adsorbed phages. Black markers, data ± SE for cells adsorbed by 2, 4, 6, 8, and 10 phages. For other MOIs, see Figure S2.

(F) Inferred parameters for the MOI-dependent model. Black markers, fitted values ± SE from bootstrapping (n = 1,030 cells, pooled from 7 independent experiments); cells at higher MOI were binned together to allow for at least 10 cells per bin. Red curves, parametrization: η and k as exponentially decaying functions of the number of adsorbed phages, τ remaining the same as in cells adsorbed by a single phage.

(G) The MOI-dependent model successfully predicts the distributions of intracellular phage numbers at a given time. Gray bars, histograms of the data, with error bars indicating SE. Red curves, model predictions. Data for cells adsorbed by 4 phages at 1, 3, 5, and 10 min are shown. For other MOIs and other time points, see Figure S2.

(legend continued on next page)

Please cite this article in press as: Nguyen et al., Coinfecting phages impede each other's entry into the cell, Current Biology (2024), https://doi.org/10.1016/j.cub.2024.05.032

of intracellular phage genomes scales sublinearly with the number of adsorbed phages (Figure 1C). To exclude the possibility that this reduced efficiency is an artifact of our capsid or genome labeling schemes, we used SYTOX orange (a DNA-intercalating dye) to visualize DNA ejection[34,35] from non-fluorescent capsids into cells that did not express fluorescent ParB fusions (Figure S1; STAR Methods). We again found that, as more phages adsorbed to the cell, the efficiency of phage ejection decreased (Figure S1). Altogether, our results thus indicate that lambda entry becomes impeded at high multiplicities of infection.

Time-lapse measurements indicate an MOI-dependent decrease in the probability and rate of phage entries

To gain insight into the observed reduction in entry efficiency, we next aimed to examine the temporal kinetics of phage entries in individual cells. To that end, we performed infection in a microfluidic device, tracking phage adsorption and entry in real time (Figure 2A; STAR Methods). The experiments provided the time series of phage adsorption and entry events in each infected cell (Figure 2A; see Figure S2 for additional cells). To interpret these time series and identify which aspect of viral entry is perturbed at high multiplicities, we formulated a simple stochastic model where phage entry is governed by three parameters (Figure 2B): η, the entry probability (at infinite time); k, the rate (or probability per unit time) of initiating entry; and τ, the time between entry initiation and detection (STAR Methods for the full model description). For a cell adsorbed by n phages, the model is solved to yield the probability distribution for the number of intracellular phage copies at time t. We first tested the model on cells adsorbed by a single phage ($n = 1$). The model successfully captured the time-dependent average number of intracellular phages $\langle \lambda(t, n = 1) \rangle$ (Figure 2C) and the distribution of phage entry time $P(T_1 | n = 1)$ (Figure 2D). The inferred parameter values ($\eta = 0.56 \pm 0.04$, $1/k = 1.7 \pm 0.2$ min, $\tau = 35.9 \pm 5.6$ s, $n = 208$ cells pooled from 7 independent experiments, SE from bootstrapping) were consistent with the entry efficiency and mean entry time we observed in bulk and with reported values[26,29,33,34,36] (Figure S1), thus lending credence to the microfluidic-acquired data and the stochastic model used to interpret it.

Having calibrated our model based on singly infected cells, we aimed to use it to predict the entry kinetics in cells adsorbed by two or more phages (Figure 2E). We first tested the null hypothesis that the parameters inferred from cells adsorbed by one phage also govern the kinetics in cells adsorbed by multiple phages ("MOI-independent model"). We found, however, that as the number of adsorbed phages increased, the prediction of intracellular phage number became poorer. In particular, the MOI-independent model overestimated the average number of intracellular phages at any given time (Figures 2E and S2). This was no surprise, considering our observations above (Figure 1C), which indicated a decrease in phages' ability to enter the cell at higher multiplicities. Aiming to capture that effect, we allowed model parameters to now vary with the number of adsorbed phages ("MOI-dependent model"). The revised model successfully reproduced the average kinetics (Figure 2E) and revealed a decrease in both entry probability η and rate k with the number of adsorbed phages per cell (Figure 2F); no MOI dependence of τ was required to capture the data (see Figure S2 for all model variations). Parametrizing η and k as exponentially decaying functions of the number of adsorbed phages, the stochastic model also captured the distributions of intracellular phage numbers at a given time (Figures 2G and S2). Finally, the model successfully reproduced the sublinear relation between the numbers of intracellular and adsorbed phages observed in both the microfluidic and bulk experiments (Figures 2H and S2). The time-lapse analysis of infection thus indicates an MOI-dependent decrease in the probability and rate of phage entries.

Phage adsorption causes cellular perturbation, resulting in impeded phage entry

How does coinfection impede phage entry into the cell? As mentioned above, the successful ejection of lambda DNA into the cell requires both LamB and PtsM.[2,19] It is conceivable that, in cells adsorbed by multiple phages, one or both of these factors become the limited resource for entry. To test this hypothesis, we performed infections of cells grown in media supplemented by either maltose or glucose (STAR Methods). The latter sugar is known to repress the expression of both LamB and PtsM,[37,38] as well as the activity of PtsM.[39] Consistent with previous reports,[37] we found that maltose-grown cells exhibited higher efficiency of lambda adsorption (Figure S3). However, no difference in entry efficiency was seen between maltose and glucose, and the same sublinear relation between the numbers of adsorbed and intracellular phages was observed in both cases (Figure S3). Our data thus suggest that LamB or PtsM levels do not drive the impedance to entry at high multiplicities.

We next asked whether the impeded entry reflects the activity of an unidentified factor produced upon early phage entries by either those phages themselves (acting as an exclusion factor[40]) or, in response to entry, by the host (as part of an anti-phage defense mechanism[41]). To test this idea, we performed infection in the presence of rifampicin, an inhibitor of transcription[42] (STAR Methods). As expected, we found that both cell growth and viral development were strongly repressed in the presence of the drug (Figure S3). However, lambda entry was not significantly impacted and exhibited the familiar reduction in efficiency as the number of adsorbed phages increased (Figure S3). We therefore concluded that impeded entry is not mediated by a factor expressed by either phage or host upon the initial viral entry.

In searching for an alternative explanation for the MOI-dependent impediment to phage entry, we revisited several reported aspects of early infection. First, phage infection induces a strong ionic perturbation to the host cell, involving fluxes of solutes and a reduction or even loss of membrane potential.[43,44] Phage-induced perturbations were reported for diverse phage and bacterial species, including lambda and *E. coli*.[43,45,46] The severity of

(H) The MOI-dependent model reproduces the sublinear relation between the numbers of adsorbed and intracellular phages. Black markers, mean ± SE; cells at higher MOI were binned together to allow for at least 10 cells per bin. Dashed line in pink, prediction by the MOI-independent model. Red curve, prediction by the MOI-dependent model. Data at 10 min following phage adsorption are shown. For other time points, see Figure S2.
See also Figure S2.

Please cite this article in press as: Nguyen et al., Coinfecting phages impede each other's entry into the cell, Current Biology (2024), https://doi.org/10.1016/j.cub.2024.05.032

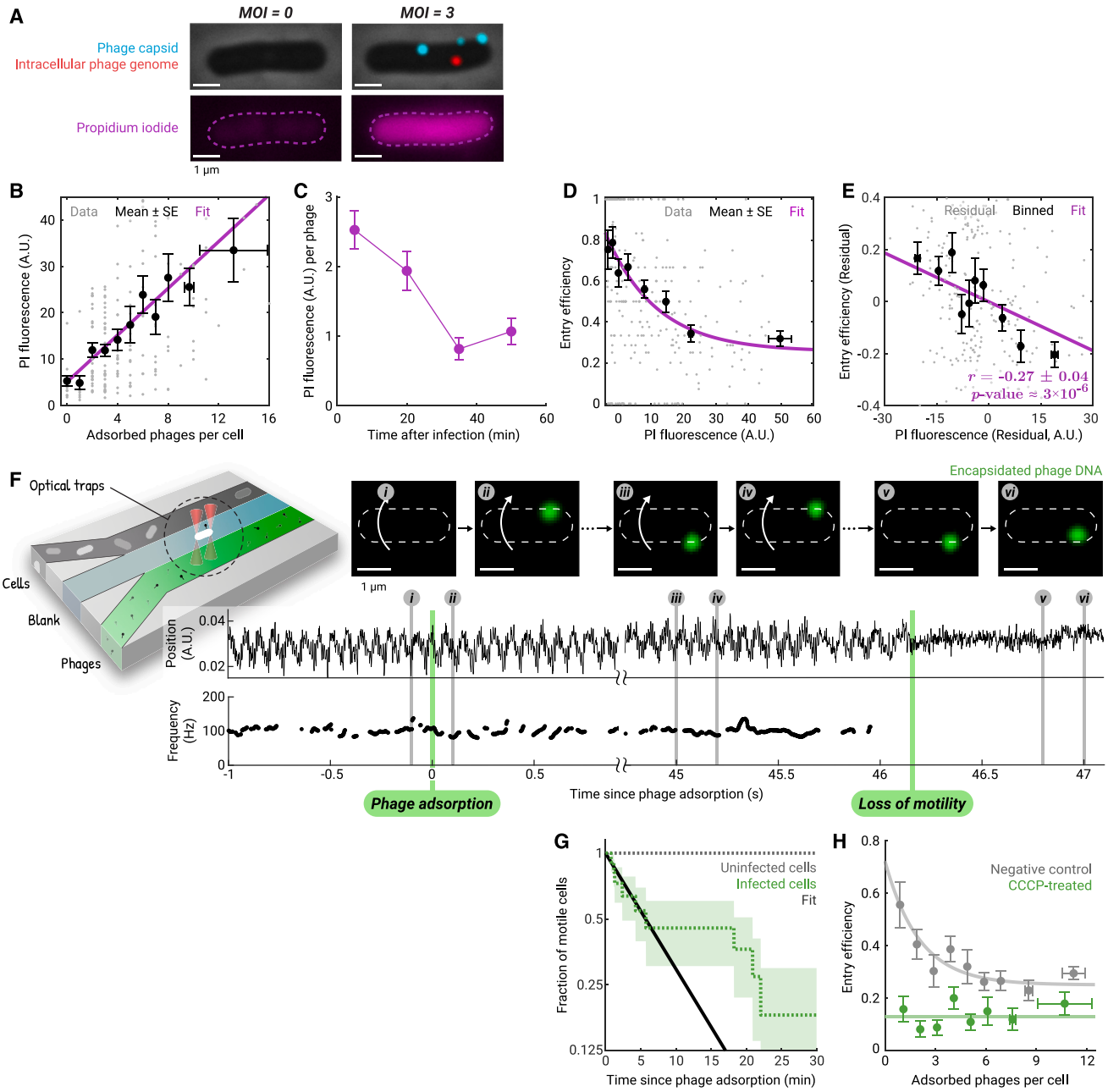

Figure 3. Phage adsorption causes cellular perturbation, resulting in impeded phage entry

(A) Following infection, cells were stained with propidium iodide (PI, shown in magenta). Dashed line, cell boundary. The image shown was taken 5 min after triggering genome ejection. Both cells were cropped from the same field of view. For additional cells, see Figure S4.

(B) Phages permeabilize the cell's membrane in an MOI-dependent manner. The intracellular fluorescence of PI is plotted as a function of the number of adsorbed phages. Gray markers, single-cell values (n = 188 cells). Black markers, mean ± SE; cells at higher MOI were binned together to allow for at least 10 cells per bin. Magenta line, linear fit, the slope of which reflects the degree of membrane permeabilization per phage. Data at 5 min after triggering genome ejection are shown. For other time points, see Figure S4.

(C) Infected cells recover membrane integrity. The slope of the linear fit between PI fluorescence and the number of adsorbed phages at each time point is plotted. Error bars indicate SE from bootstrapping (n = 188, 132, 131, and 135 cells).

(D) The efficiency of phage entry decreases in cells with stronger PI fluorescence. Gray markers, single-cell values (n = 298 cells pooled from t = 5 and 20 min). Black markers, mean ± SE (40 cells per bin). Magenta curve, fit to an exponential decay with a baseline.

(E) Phage entry efficiency and PI fluorescence, conditioned on the number of adsorbed phages, are negatively correlated. Gray markers, residuals obtained by linear regression of the PI fluorescence and of the entry efficiency on the number of adsorbed phages (n = 298 cells). Black markers, mean ± SE of the residuals (30 cells per bin). Magenta line, linear fit.

(F) The flagellar rotation frequency of phage-infected cells, indicating the membrane potential, is measured using optical traps. Top left: schematic of the trap setup and the flow chamber. Top right: a trapped cell with one adsorbed phage (encapsidated DNA was stained using SYTOX orange, shown in green), imaged

(legend continued on next page)

Please cite this article in press as: Nguyen et al., Coinfecting phages impede each other's entry into the cell, Current Biology (2024), https://doi.org/10.1016/j.cub.2024.05.032

perturbation increases with MOI[45,47] but does not always require phage entry to occur, as evidenced by infection of "ghost" phage particles devoid of DNA.[47–49] Could these perturbations to the host cell underlie the diminished entry we find at higher MOI? Consistent with this idea, ionic conditions have been shown to impact the kinetics of DNA ejection *in vitro*,[12] possibly by modulating the self-repulsion of the encapsidated DNA or altering the osmotic pressure that opposes ejection.[12] In lambda, specifically, both the extent[50–52] and rate[53,54] of DNA ejection are affected. Putting these elements together, we hypothesized that phage-induced perturbations to the host physiology, which occur following adsorption but prior to entry, impede phage entry into the cell in an MOI-dependent manner.

To directly probe the relation between phage-induced perturbation and DNA entry, we focused on two reported aspects of this perturbation: the compromise to membrane integrity and the reduction of membrane potential.[12] To measure the membrane integrity, we performed infection in LB supplemented with maltose and $MgSO_4$, sampled the infection mixture at different times, and stained cells using propidium iodide (PI; STAR Methods). For each cell, we recorded the numbers of adsorbed and intracellular phages, as well as the intracellular PI fluorescence (Figure 3A; see Figure S4 for additional cells). Within 5 min of infection, cells became permeable to PI, with intracellular PI fluorescence rising linearly with the number of adsorbed phages (Figure 3B). The MOI dependence of permeability is consistent with the idea that each adsorbed phage induces an opening in the cell membrane.[47,55] In agreement with reports that phage-induced perturbations do not require entry,[47,49] we found that PI permeation was not correlated with the intracellular phage numbers (Figure S4). We note that the permeation of PI into phage-infected cells did not reflect cell death or phage-induced lysis, and PI-stained cells still exhibited the sublinear relation between the numbers of adsorbed and intracellular phages (STAR Methods; Figure S4). Examining PI fluorescence later in infection, we found that the degree of PI permeation per adsorbed phage decreased over time, indicating that the infected cells gradually recover membrane integrity (Figure 3C). Taken together, these results show that phage adsorption transiently permeabilizes the infected cell's membrane in an MOI-dependent manner.

We next used the degree of PI permeation to test whether the compromise to membrane integrity impedes phage entry. Examining single-cell data up to 20 min post-infection (prior to the recovery of membrane integrity; Figure 3C), we found that cells with stronger PI fluorescence exhibited lower efficiency of phage entry (ratio of intracellular phage genomes to adsorbed phages per cell; Figure 3D). In particular, the entry efficiencies found in the least and most permeabilized cells were comparable to the values observed above for cells with low and high numbers of adsorbed phages, respectively (Figure 1C). Although these findings are consistent with the idea that the impediment to entry reflects the severity of the phage-induced perturbation, the observed correlation is vulnerable to the confounding effect of the number of adsorbed phages per cell, which is correlated with both the efficiency of phage entry (Figure 1C) and the intracellular PI fluorescence (Figure 3B). To directly establish the causal link between PI permeation and entry, we applied causal inference[56] by calculating the correlation between entry efficiency and PI fluorescence, conditioned on the number of adsorbed phages (STAR Methods; Figure S4). Consistent with our hypothesis, the correlation coefficient r(entry efficiency, PI fluorescence|number of adsorbed phages) was still negative (Figure 3E). Although we cannot rule out the presence of additional mechanisms connecting phage adsorption and impeded entry,[56] our causal inference analysis established that phage-induced compromise to membrane integrity is a cause of entry impediment.

To examine phage-induced changes to *E. coli*'s membrane potential, we utilized as proxies the flagellar rotation frequency[57] and the fluorescence of a proteo-rhodopsin optical proton sensor (PROPS),[58] both of which vary with the proton motive force. We used dual-trap optical tweezers to trap cells in a flow chamber, into which chemicals and phages can be perfused.[59] Trapped cells were fluorescently imaged, while their flagellar rotation frequency was inferred from the trap signal[60] (Figure 3F; STAR Methods). Exposing cells to carbonyl cyanide *m*-chlorophenyl hydrazone (CCCP), a protonophore that depletes the proton motive force,[58] resulted in rapid loss of flagellar motility and an increase in fluorescence from PROPS (Figure S5), as expected. A similar cessation of motility was exhibited following lambda adsorption (Figures 3F and 3G; Video S1). The typical time for an infected cell to lose motility—indicated by the half-life of the exponential fit in Figure 3G (5.7 ± 2.7 min; n = 11 cells, SE from bootstrapping)—was consistent with the timescale of ionic fluxes from lambda-infected cells (Figure S5).[43,46] The encapsidated DNA of the adsorbed phages could still be detected on cells that had lost motility (Figure 3F; Video S1), indicating that membrane depolarization did not require phage entry. Phage-induced depolarization was also revealed by the changes to PROPS fluorescence, which mirrored the effect of CCCP treatment (Figure S5).

Having established that lambda adsorption results in membrane depolarization, we next aimed to test whether membrane depolarization will in turn impede entry. To do so, we measured entry efficiency in cells treated with 200 μM CCCP (a concentration that induces a complete loss of membrane potential [Figure S5] and results in a similar degree of PI permeation to that

over time; the dashed line indicates the cell outline, and the white arrow indicates the cell body rotation. Bottom right: the trapped cell position and the flagellar rotation frequency of the same cell; gray vertical lines indicate the time points corresponding to the snapshots. See also Video S1.

(G) Phage adsorption results in loss of motility. Dotted green line, the fraction of motile cells following phage adsorption (MOI = 1), with shading for SE (n = 11 cells). Black line, exponential fit to the data up to 10 min. Dotted gray line, the fraction of motile cells in the uninfected sample (n = 7 cells).

(H) Complete membrane depolarization results in impeded phage entry. Green markers, mean (± SE) entry efficiency of cells depolarized using carbonyl cyanide *m*-chlorophenyl hydrazone (CCCP, n = 219 cells). Green line, the average over all cells in the CCCP-treated sample. Gray markers, mean ± SE for cells treated with 0.5% DMSO, serving as a negative control (n = 209 cells). Gray line, fit to an exponential decay with a baseline. For both samples, cells at higher MOI are binned together to allow for at least 5 cells per bin.

See also Figures S3–S5.

Please cite this article in press as: Nguyen et al., Coinfecting phages impede each other's entry into the cell, Current Biology (2024), https://doi.org/10.1016/j.cub.2024.05.032

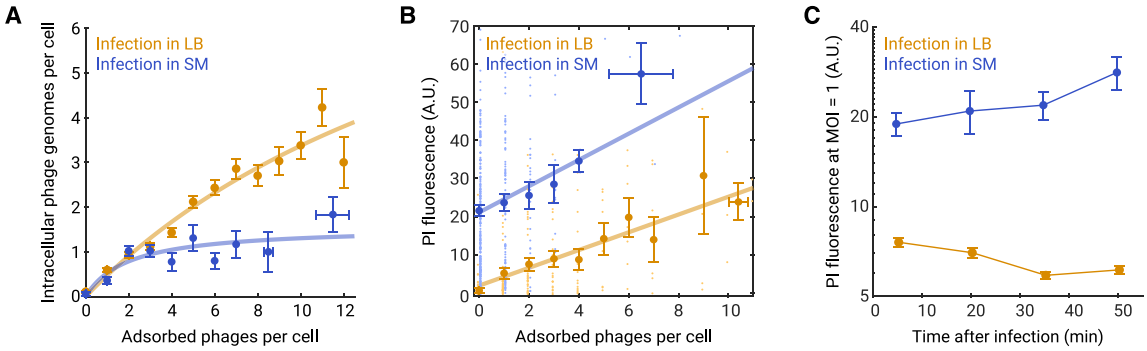

Figure 4. The infection medium modulates the extent of entry impediment

(A) Infection media alter the degree to which lambda entry is impeded. Identically cultured cells were infected in different media, and the numbers of adsorbed and intracellular phages per cell were measured at 5 min after triggering genome ejection. Orange markers, mean ± SE for infection in LB (data reproduced from Figure 1C). Blue markers, infection in SM (n = 242 cells, at least 5 cells per bin). Orange and blue curves, fit to a Michaelis-Menten function. For other infection media and buffers, see Figure S6.

(B) Membrane permeabilization in SM is more severe than that in LB. Light blue and light orange markers, single-cell values for the intracellular fluorescence of propidium iodide (PI) as a function of the number of adsorbed phages in the same cell, measured at 5 min after triggering genome ejection (n = 217 and 431 cells for LB and SM, respectively). Blue and orange markers, mean ± SE; cells at higher MOI were binned together to allow for at least 5 cells per bin. Blue and orange lines, linear fits.

(C) Membrane permeabilization in SM is longer-lasting than that in LB. The PI fluorescence in cells adsorbed by one phage (MOI = 1) was inferred from linear fitting of PI fluorescence as a function of the number of adsorbed phages, measured at different time points after triggering genome ejection. Orange markers, infection in LB (same time series data as shown in Figure S4). Blue markers, infection in SM (n = 261, 234, 190, and 184 cells at 5, 20, 35, and 50 min, respectively). Error bars indicate SE from bootstrapping.

See also Figure S6.

of lambda-infected cells [Figure S4]). Although intracellular lambda genomes were still detected following CCCP treatment, the entry efficiency (~15%, n = 219 cells) was lower than that of untreated cells (Figure 3H) and comparable to the value in (untreated) cells with high numbers of adsorbed phages (Figures 1C, 2F, and 3H). Depolarization-induced entry efficiency was also similar to that of highly permeabilized cells, as indicated by PI fluorescence (Figure 3D). Thus, CCCP-induced membrane depolarization emulates the perturbation caused by adsorption of multiple phages and results in significantly impeded phage entry.

The infection medium modulates the extent of entry impediment

Previous studies in several phages have shown that the severity and duration of phage-induced ionic perturbations strongly depend on the medium in which infection takes place.[61,62] In light of our finding that these perturbations underlie the MOI-dependent entry impediment, we reasoned that varying infection conditions would also result in different entry characteristics. To test this prediction, we grew cells in LB, supplemented with maltose and $MgSO_4$, and performed infection in 11 different solutions used in microbiological studies (STAR Methods). This survey revealed diverse relations between the numbers of adsorbed and intracellular phages (Figure S6). Some infection conditions, including LB, tryptone broth (TB), and M9 minimal media, permit multiple phage entries (Figure S6). However, under other conditions, such as saline magnesium (SM, a common phage buffer[63]), phosphate-buffered saline (PBS), and trap motility buffer (used in the optical trap assay[60]), adsorption by as many as ten or more phages only resulted, on average, in a single phage entry (Figure S6).

Taking SM as a representative of conditions where phage entry is severely impeded (Figure 4A), we confirmed that the compromise to the cell membrane in SM, measured using PI (STAR Methods), was more severe than that in LB (Figure 4B). Notably, the PI fluorescence in cells adsorbed by a single phage in SM was comparable to that induced by ~10 phages in LB (Figure 4B), at which point phage entry was strongly impeded. Furthermore, in contrast to LB where the PI fluorescence of singly adsorbed cells decreased over time (recall Figure 3C), the signal in SM *increased* (Figure 4C), suggesting that the phage-adsorbed cells in SM remain permeabilized at later times. Taken together, these results are consistent with the picture where the extent of entry impediment reflects the degree of phage-induced, medium-dependent perturbations.

Impediment to viral entry impacts the infection outcome

In nature, the occurrence of lysogeny is reported to vary greatly with the environmental conditions.[64,65] Motivated by the survey of infection media above (Figure S6), we hypothesized that the environmental conditions exert their influence on lysogeny, at least in part, by setting different limits on the intracellular phage number, which in turn drives the choice of developmental program by the phage.[8] To test this hypothesis, we assayed the frequency of lysogeny when infection takes place in the two media characterized above (Figure 4): LB (which enables multiple phage entries) and SM (which limits entry to a single phage, on average). In both cases, cell growth pre- and post-infection took place in LB,[8] and cells were not starved prior to infection (STAR Methods). Following Yao et al.[8], we again used a replication-deficient phage, where the number of viral genomes remains constant following entry. Under each infection condition, we measured the fraction of cells undergoing lysogeny as a

Please cite this article in press as: Nguyen et al., Coinfecting phages impede each other's entry into the cell, Current Biology (2024), https://doi.org/10.1016/j.cub.2024.05.032

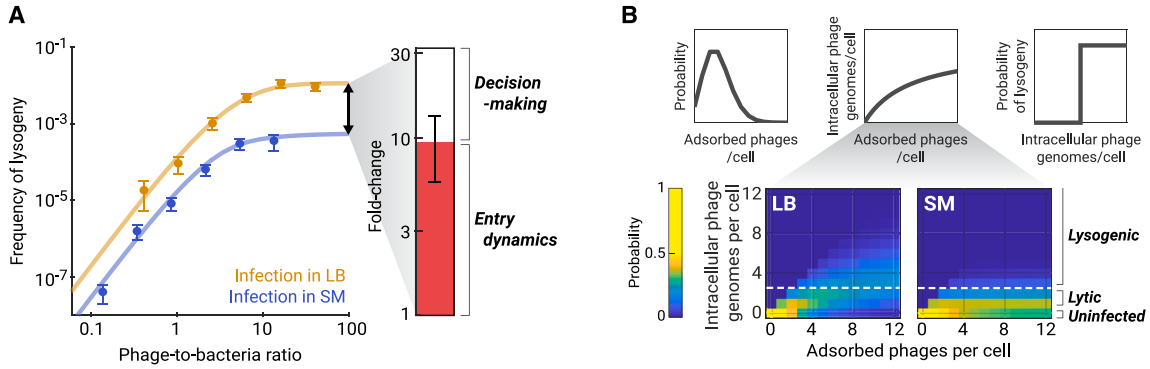

Figure 5. Impediment to viral entry impacts the infection outcome

(A) Entry dynamics in different media accounts for most of the difference in lysogenization frequency. Left: the frequencies of lysogeny as a function of phage-to-bacteria ratios (corrected for adsorption efficiency) when infection is performed in LB (orange) and SM (blue). Markers, mean ± SE from technical duplicates. Orange and blue curves, fit to the model in (B). Right: entry dynamics (red) accounts for ~10-fold of the observed ~30-fold difference in the maximum frequency of lysogeny between the two media. The other ~3-fold is due to differences in the single-cell probability of lysogeny (white, SE from bootstrapping).

(B) Schematic of the model used to capture the data in (A). Top: the model accounts for phage adsorption, entry, and decision-making. Bottom: the predicted distributions of intracellular phage numbers in LB and SM, parametrized using the data in Figure 4A. Dashed lines, the minimum MOI required for lysogenization. See also Figure S7 and Table S6.

function of the phage-to-bacteria ratio (Figure S7).[66] The two conditions resulted in distinct lysogeny-versus-MOI curves (Figure 5A). In particular, at higher ratios of phage to bacteria, when cells are likely absorbed by multiple phages, the frequency of lysogeny in SM saturated at a value ~30-fold lower than that in LB. Thus, given the same growth and recovery conditions, the choice of infection conditions dramatically impacted the propensity to lysogenize at high MOI.

We interpreted the lysogenization curves in the two media using a simple model (Figure 5B) consisting of (1) random phage-bacteria collisions, resulting in a Poisson distribution of single-cell numbers of adsorbed phages[8]; (2) stochastic entry of phages into the cell, parametrized using the experimentally measured values (Figures 4A and S6); and (3) choice of lysogeny if three or more phage genomes entered the cell[5,8] (STAR Methods). The model was able to capture the experimental curves (Figure 5A). The inferred model parameters revealed that the difference in phage entry—specifically, the reduced probability in SM of having three or more intracellular phages, even at high numbers of adsorbed phages—accounted for most of the difference in lysogenization between the two media (Figure 5A). In other words, when infecting in SM, the number of intracellular phage genomes poorly reflected the phage-to-bacteria ratio in the environment, resulting in a strong impact on infection outcome.

Protracted viral entry increases the heterogeneity in cell fate

Finally, beyond its impact on the lysogeny phenotype as measured in bulk (Figure 5), we asked whether entry dynamics can account for the reported cell-to-cell variability in infection outcome at a given MOI.[6,67,68] Although this heterogeneity has traditionally been attributed to the stochastic ("noisy") expression of genes in the decision network,[69] the idea lacks experimental evidence. We reasoned that, instead, the stochastic kinetics of phage entry may be key. This was motivated by recent works suggesting that, rather than simply measuring MOI, the lysis/lysogeny decision circuit weighs intracellular genomes by their arrival times, with latecomers contributing less to the outcome.[8,32] To test the consequences of stochastic entry, we first used our entry model (Figure 2B) to create simulated time series of phage entries in many individual cells, under varying numbers of adsorbed phages (STAR Methods). We then used this series as the input to a deterministic model of the decision network,[8] yielding the predicted kinetics for the concentrations of the Cro and CI transcription factors, and thus the infection outcome, in each cell (Figure 6A; see Figure S7 for additional MOIs). To facilitate comparison with the single-cell data of Zeng et al.,[6] we simulated infection by a replication-competent (wild-type) phage. When stochastic entry dynamics are ignored, i.e., all adsorbed phages are assumed to enter the cell instantaneously, cells adsorbed by two phages show dominant CI expression, resulting in the choice of lysogeny[8] (Figure 6A). By contrast, when entry dynamics is incorporated into the model, some cells adsorbed by two phages may have only one intracellular phage genome, or the second phage genome may arrive in the cell too late to contribute to the decision.[8,32] As a result, approx. 50% of the infected cells are Cro-dominant and will hence undergo lysis (Figure 6A; see Figure S7 for infection outcomes at other MOIs).

To quantify the heterogeneity in infection outcome, we calculated the resulting "decision curve," which describes the fraction of cells undergoing lysogeny as a function of single-cell MOI—here taken as the number of phages adsorbed to the cell, the observable in Zeng et al.[6] When entry dynamics were incorporated into the model, the predicted decision curve increased gradually rather than step-like, reminiscent of the data in Zeng et al.[6] (Figure 6B). The degree of precision of the decision can be quantified using the fitted Hill coefficient of this curve.[6,70] We found that incorporating entry dynamics into the model reduced the Hill coefficient from 7.9 ± 0.4 to 1.8 ± 0.1 (Figure 6B), thus considerably closer to the experimental value of 1.0 ± 0.1 in Zeng et al.[6] The "flattening" of the step-like response present in the original model[8] reflects the lower entry efficiency and slower

Please cite this article in press as: Nguyen et al., Coinfecting phages impede each other's entry into the cell, Current Biology (2024), https://doi.org/10.1016/j.cub.2024.05.032

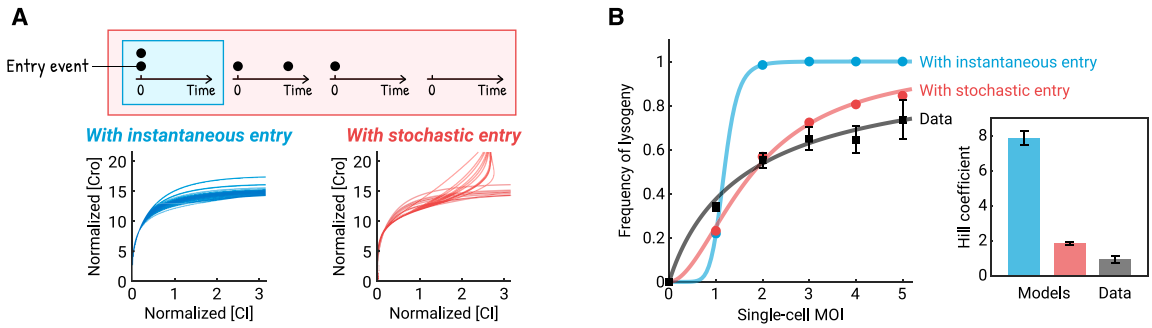

Figure 6. Protracted viral entry increases the heterogeneity in cell fate

(A) Stochastic phage entry results in different expression profiles of Cro (driving lysis) and CI (driving lysogeny). Top: schematics of the temporal change in the number of intracellular phage genomes in cells adsorbed by two phages, assuming instantaneous (cyan) or stochastic (red) phage entry. Bottom: predicted single-cell trajectories of Cro and CI concentrations in the Yao et al.[8] model, assuming different dynamics of phage entry. Trajectories of 24 cells, each adsorbed by two phages, are shown for each case. For other MOIs, see Figure S7.

(B) Entry dynamics increase the cell-to-cell variability in infection outcome at a given MOI. Black markers, data from Zeng et al.[6] Cyan and red markers, predictions by the model of Yao et al. in the absence or presence of stochastic entry kinetics, respectively. Solid curves, fits to Hill functions. The Hill coefficients, which describe the degree of precision in the lysis versus lysogeny decision, are shown on the right (SE from bootstrapping).

See also Figure S7.

entry in cells adsorbed by multiple phages. That this effect is captured by a fully deterministic model of the decision suggests a diminished role for stochastic gene expression in explaining the observed heterogeneity of outcome among cells.

Phages T5 and P1 exhibit MOI- and medium-dependent impediment to cell entry

Considering that phage-induced perturbations and ion-modulated ejection have been reported for multiple phage-bacteria systems,[12] we hypothesized that the MOI-dependent entry we found extends beyond lambda. We tested this hypothesis in two phages: T5, a virulent phage of the same *Siphoviridae* family as lambda, and P1, a temperate phage of the *Myoviridae* family. Motivating our choice, infections by both T5 and P1 have been reported to induce ionic fluxes and/or membrane depolarization.[43,71] To measure the efficiency of phage entry, we utilized the SYTOX orange assay (used above in lambda; Figure S1) and tracked the disappearance of fluorescently labeled encapsidated DNA in cells adsorbed by varying numbers of phages (Figure 7; STAR Methods). Mirroring the observation in lambda (Figures 1C and S1), we found that entry efficiency in both T5 and P1 decreased with the number of adsorbed phages (Figure 7). As in lambda (Figures 4A and S1), phage P1 exhibited lower entry efficiencies in SM than in LB (Figure 7). We were unable to quantify the entry efficiency of T5 in LB since some cells in the infected sample were already damaged—likely due to phage entry—by the time imaging began. This observation nevertheless suggested that T5 entry in LB was faster than that in SM. Taken together, these findings suggest that MOI-dependent impediment to entry, modulated by the infection medium, may be a general phenomenon.

DISCUSSION

Above, we provided evidence that phage-induced perturbations to the host cell impede DNA entry at high multiplicities of infection. However, the molecular details of this phenomenon remain unknown. Elucidating those details will contribute, we believe, to a deeper understanding of how phage entry takes place, including the forces driving DNA translocation and the structural changes to both phage particle and cell envelope during the entry process. Already, by highlighting the intimate relation between viral entry and the host's membrane integrity and ionic balance, our findings contribute to the emerging view of electrophysiology as a prime mover in the bacterial cell,[72] adding a role in phage infection to recent discoveries implicating electrophysiology in microbial stress response and biofilm formation.[73] More generally, our findings demonstrate yet again the importance of examining physiological processes in their native, *in vivo* context, where the full complexity of the cellular environment results in regulatory interactions absent from *in vitro* experiments.

The dynamics of viral entry, as described in this work, have important implications for the outcome of bacteriophage infection. For temperate phages, the strong dependence on medium conditions provides a way for the environment to impact the choice of cell fate by modulating the timing and number of phage genomes entering the cell. This previously unappreciated effect may help resolve the standing conflict between the simple MOI-to-lysogeny mapping observed in the lab and the complex, sometimes contradictory, relations found in natural phage habitats.[74–76] Beyond the case of infection by multiple copies of the same phage, mutual impedance of entry may facilitate competition between phages of different species that coinfect the same host,[77] where the effect may be seen as an alternative form of superinfection exclusion,[40,41] one that does not entail gene expression from the internalized phage genomes.

Finally, the stochastic and protracted entry of coinfecting phages may also have implications for the continuous arms race between phages and bacteria.[40,41] From the point of view of the infected cell, the sensitivity of phage entry to physiological parameters may provide an opportunity for the host to delay a critical step in the infection cycle, while its defenses are triggered,[46,78,79] and offers regulatory opportunities to halt this entry altogether. The reverse is that delayed entries may

Please cite this article in press as: Nguyen et al., Coinfecting phages impede each other's entry into the cell, Current Biology (2024), https://doi.org/10.1016/j.cub.2024.05.032

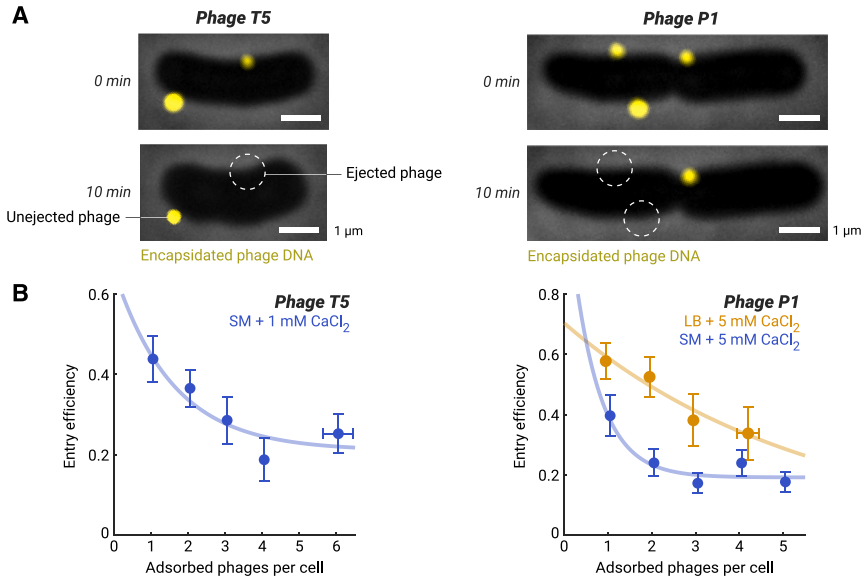

Figure 7. Phages T5 and P1 exhibit MOI- and medium-dependent impediment to cell entry

(A) *E. coli* cells infected by phages whose encapsidated DNA was fluorescently labeled using SYTOX orange (yellow signal). Left: infection by T5. Right: infection by P1. Dashed circles, the disappearance of SYTOX orange spots between 0 and 10 min was interpreted as ejection of the encapsidated DNA.

(B) Entry efficiency of phages T5 and P1 is reduced in cells adsorbed by multiple phages. Orange markers, mean ± SE for infection in LB (n = 234 cells for P1). Blue markers, mean ± SE for infection in SM (n = 256 and 221 cells for T5 and P1, respectively). For all samples, cells at higher MOI were binned together to allow for at least 5 cells per bin. Orange and blue curves, fits to an exponential decay with a baseline, serving as a guide to the eye. Both LB and SM were supplemented with $CaCl_2$, required for successful T5 and P1 infection.

facilitate cooperation between coinfecting phages, with early-arriving phages counteracting the host's defense system,[78,80] allowing later-arriving phages to survive and successfully propagate.[81]

STAR★METHODS

Detailed methods are provided in the online version of this paper and include the following:

- KEY RESOURCES TABLE
- RESOURCE AVAILABILITY
  - Lead contact
  - Materials availability
  - Data and code availability
- EXPERIMENTAL MODEL AND SUBJECT DETAILS
  - Bacterial strains, phages, and plasmids
  - Chemical reagents, growth media, and buffers
  - Phage preparation
  - Bacterial growth conditions
- METHOD DETAILS
  - Measuring the numbers of adsorbed phages and intracellular phage genomes following bulk infection
  - Measuring the efficiency of phage entry using SYTOX Orange
  - Measuring phage-induced membrane permeabilization using propidium iodide
  - Measuring the time of the first phage entry following bulk infection
  - Measuring the kinetics of phage entries in the microfluidic device
  - Validating the ParB-*parS* labeling system using SYTOX Orange
  - Validating the CCCP treatment protocol using PROPS
  - Microscopy
  - Image analysis
  - Optical trap assay
  - Preparation of representative images
  - Potassium efflux assay
  - Measuring the frequency of lysogeny following infection in different media
  - Modeling bulk lysogenization following phage entry in different media
  - Stochastic model of phage entry kinetics
  - Simulating the stochastic model
  - Stochastic simulation of infection outcome in individual cells
- QUANTIFICATION AND STATISTICAL ANALYSIS

SUPPLEMENTAL INFORMATION

Supplemental information can be found online at https://doi.org/10.1016/j.cub.2024.05.032.

ACKNOWLEDGMENTS

We are grateful to the following people for their generous advice: M. Gruebele, M. Goulian, C. Herman, K. Maxwell, I. Molineux, T. Pilizota, A. Sokac, K. Venken, T. Wensel, Z. Yu, C. Zong, and all members of the Golding lab. Work in the Golding lab is supported by the National Institutes of Health grant R35 GM140709, the National Science Foundation grant 2243257 (NSF Science and Technology Center for Quantitative Cell Biology), and the Alfred P. Sloan Foundation under grant G-2023-19649. Work in the Chemla lab is supported by the National Science Foundation Physics Frontiers Center (PFC) "Center for the Physics of Living Cells" (CPLC) grant PHY 1430124 and the National Institutes of Health grant R35 GM144125. Work in the Zeng lab is supported by the National Science Foundation grant MCB 2013762. We gratefully acknowledge the computing resources provided by the Computational and Integrative Biomedical Research Center of Baylor College of Medicine.

AUTHOR CONTRIBUTIONS

Conceptualization, T.V.P.N. and I.G.; methodology, T.V.P.N., Y.W., T.Y., J.T.T., L.Z., Y.R.C., and I.G.; investigation and formal analysis, T.V.P.N., Y.W., Y.R.C., and I.G.; visualization, T.V.P.N.; writing – original draft, T.V.P.N. and I.G.; writing – review & editing, T.V.P.N., L.Z., Y.R.C., and I.G.; funding acquisition and supervision, L.Z., Y.R.C., and I.G.; project administration, I.G.

DECLARATION OF INTERESTS

The authors declare no competing interests.

Received: August 11, 2023
Revised: February 15, 2024
Accepted: May 16, 2024
Published: June 14, 2024

REFERENCES

1. Oppenheim, A.B., Kobiler, O., Stavans, J., Court, D.L., and Adhya, S. (2005). Switches in bacteriophage lambda development. Annu. Rev. Genet. *39*, 409–429.
2. Casjens, S.R., and Hendrix, R.W. (2015). Bacteriophage lambda: early pioneer and still relevant. Virology *479–480*, 310–330.
3. Ofir, G., and Sorek, R. (2018). Contemporary phage biology: from classic models to new insights. Cell *172*, 1260–1270.
4. Shao, Q., Trinh, J.T., and Zeng, L. (2019). High-resolution studies of lysis–lysogeny decision-making in bacteriophage lambda. J. Biol. Chem. *294*, 3343–3349.
5. Kourilsky, P. (1973). Lysogenization by bacteriophage lambda. I. Multiple infection and the lysogenic response. Mol. Gen. Genet. *122*, 183–195.
6. Zeng, L., Skinner, S.O., Zong, C., Sippy, J., Feiss, M., and Golding, I. (2010). Decision making at a subcellular level determines the outcome of bacteriophage infection. Cell *141*, 682–691.
7. Weitz, J.S., Mileyko, Y., Joh, R.I., and Voit, E.O. (2008). Collective decision making in bacterial viruses. Biophys. J. *95*, 2673–2680.
8. Yao, T., Coleman, S., Nguyen, T.V.P., Golding, I., and Igoshin, O.A. (2021). Bacteriophage self-counting in the presence of viral replication. Proc. Natl. Acad. Sci. USA *118*, e2104163118.
9. Golding, I., Coleman, S., Nguyen, T.V.P., and Yao, T. (2020). Decision making by temperate phages. In Encyclopedia of Virology, Fourth Edition, *1–5*, D.H. Bamford, and M.B.T. Zuckerman, eds. (Academic Press), pp. 88–97.
10. Duddy, O.P., and Bassler, B.L. (2021). Quorum sensing across bacterial and viral domains. PLoS Pathog. *17*, e1009074.
11. Golding, I. (2018). Infection by bacteriophage lambda: an evolving paradigm for cellular individuality. Curr. Opin. Microbiol. *43*, 9–13.
12. Molineux, I.J., and Panja, D. (2013). Popping the cork: mechanisms of phage genome ejection. Nat. Rev. Microbiol. *11*, 194–204.
13. Chen, Y.J., Wu, D., Gelbart, W., Knobler, C.M., Phillips, R., and Kegel, W.K. (2018). Two-stage dynamics of in vivo bacteriophage genome ejection. Phys. Rev. X *8*, 021029.
14. Lemay, S.G., Panja, D., and Molineux, I.J. (2013). Role of osmotic and hydrostatic pressures in bacteriophage genome ejection. Phys. Rev. E Stat. Nonlin. Soft Matter Phys. *87*, 022714.
15. Schwartz, M. (1975). Reversible interaction between coliphage lambda and its receptor protein. J. Mol. Biol. *99*, 185–201.
16. Rothenberg, E., Sepúlveda, L.A., Skinner, S.O., Zeng, L., Selvin, P.R., and Golding, I. (2011). Single-virus tracking reveals a spatial receptor-dependent search mechanism. Biophys. J. *100*, 2875–2882.
17. Roa, M., and Scandella, D. (1976). Multiple steps during the interaction between coliphage lambda and its receptor protein in vitro. Virology *72*, 182–194.
18. Berrier, C., Bonhivers, M., Letellier, L., and Ghazi, A. (2000). High-conductance channel induced by the interaction of phage lambda with its receptor maltoporin. FEBS Lett. *476*, 129–133.
19. Wang, C., Duan, J., Gu, Z., Ge, X., Zeng, J., and Wang, J. (2024). Architecture of the bacteriophage lambda tail. Structure *32*, 35–46.e3.
20. Roessner, C.A., and Ihler, G.M. (1984). Proteinase sensitivity of bacteriophage lambda tail proteins gpJ and pH in complexes with the lambda receptor. J. Bacteriol. *157*, 165–170.
21. Esquinas-Rychen, M., and Erni, B. (2001). Facilitation of bacteriophage lambda DNA injection by inner membrane proteins of the bacterial phosphoenol-pyruvate: carbohydrate phosphotransferase system (PTS). J. Mol. Microbiol. Biotechnol. *3*, 361–370.
22. Cumby, N., Reimer, K., Mengin-Lecreulx, D., Davidson, A.R., and Maxwell, K.L. (2015). The phage tail tape measure protein, an inner membrane protein and a periplasmic chaperone play connected roles in the genome injection process of E. coli phage HK97. Mol. Microbiol. *96*, 437–447.
23. Scandella, D., and Arber, W. (1974). An Escherichia coli mutant which inhibits the injection of phage λ DNA. Virology *58*, 504–513.
24. Elliott, J., and Arber, W. (1978). E. coli K-12 pel mutants, which block phage λ DNA injection, coincide with ptsM, which determines a component of a sugar transport system. Mol. Gen. Genet. *161*, 1–8.
25. Scandella, D., and Arber, W. (1976). Phage λ DNA injection into Escherichia coli pel– mutants is restored by mutations in phage genes V or H. Virology *69*, 206–215.
26. Shao, Q., Hawkins, A., and Zeng, L. (2015). Phage DNA dynamics in cells with different fates. Biophys. J. *108*, 2048–2060.
27. Nielsen, H.J., Youngren, B., Hansen, F.G., and Austin, S. (2007). Dynamics of Escherichia coli chromosome segregation during multifork replication. J. Bacteriol. *189*, 8660–8666.
28. Tal, A., Arbel-Goren, R., Costantino, N., Court, D.L., and Stavans, J. (2014). Location of the unique integration site on an Escherichia coli chromosome by bacteriophage lambda DNA in vivo. Proc. Natl. Acad. Sci. USA *111*, 7308–7312.
29. Mackay, D.J., and Bode, V.C. (1976). Events in lambda injection between phage adsorption and DNA entry. Virology *72*, 154–166.
30. Dennehy, J.J., and Abedon, S.T. (2020). Adsorption: phage acquisition of bacteria. In Bacteriophages (Springer), pp. 1–25.
31. Moldovan, R., Chapman-McQuiston, E., and Wu, X.L. (2007). On kinetics of phage adsorption. Biophys. J. *93*, 303–315.
32. Cortes, M.G., Trinh, J.T., Zeng, L., and Balázsi, G. (2017). Late-arriving signals contribute less to cell-fate decisions. Biophys. J. *113*, 2110–2120.
33. Guan, J., Ibarra, D., and Zeng, L. (2019). The role of side tail fibers during the infection cycle of phage lambda. Virology *527*, 57–63.
34. Van Valen, D., Wu, D., Chen, Y.J., Tuson, H., Wiggins, P., and Phillips, R. (2012). A single-molecule Hershey-Chase experiment. Curr. Biol. *22*, 1339–1343.
35. Tzipilevich, E., Habusha, M., and Ben-Yehuda, S. (2017). Acquisition of phage sensitivity by bacteria through exchange of phage receptors. Cell *168*, 186–199.e12.
36. García, L.R., and Molineux, I.J. (1995). Rate of translocation of bacteriophage T7 DNA across the membranes of Escherichia coli. J. Bacteriol. *177*, 4066–4076.
37. Schwartz, M. (1976). The adsorption of coliphage lambda to its host: effect of variations in the surface density of receptor and in phage-receptor affinity. J. Mol. Biol. *103*, 521–536.
38. Plumbridge, J. (1998). Control of the expression of the manXYZ operon in Escherichia coli: Mlc is a negative regulator of the mannose PTS. Mol. Microbiol. *27*, 369–380.
39. Fraser, A.D.E., and Yamazaki, H. (1983). Regulatory relationship between PTSM and PTSG in Escherichia coli. FEMS Microbiol. Lett. *16*, 61–63.
40. Labrie, S.J., Samson, J.E., and Moineau, S. (2010). Bacteriophage resistance mechanisms. Nat. Rev. Microbiol. *8*, 317–327.
41. Hampton, H.G., Watson, B.N.J., and Fineran, P.C. (2020). The arms race between bacteria and their phage foes. Nature *577*, 327–336.
42. Wang, M., Zhang, J., Xu, H., and Golding, I. (2019). Measuring transcription at a single gene copy reveals hidden drivers of bacterial individuality. Nat. Microbiol. *4*, 2118–2127.
43. Kuhn, A., and Kellenberger, E. (1985). Productive phage infection in Escherichia coli with reduced internal levels of the major cations. J. Bacteriol. *163*, 906–912.
44. Letellier, L., Plançon, L., Bonhivers, M., and Boulanger, P. (1999). Phage DNA transport across membranes. Res. Microbiol. *150*, 499–505.
45. Kourilsky, P., and Knapp, A. (1974). Lysogenization by bacteriophage lambda. III. Multiplicity dependent phenomena occuring upon infection by lambda. Biochimie *56*, 1517–1523.
46. Kronheim, S., Daniel-Ivad, M., Duan, Z., Hwang, S., Wong, A.I., Mantel, I., Nodwell, J.R., and Maxwell, K.L. (2018). A chemical defence against phage infection. Nature *564*, 283–286.

47. Boulanger, P., and Letellier, L. (1988). Characterization of ion channels involved in the penetration of phage T4 DNA into Escherichia coli cells. J. Biol. Chem. *263*, 9767–9775.

48. Duckworth, D.H. (1970). Biological activity of bacteriophage ghosts and "take-over" of host functions by bacteriophage. Bacteriol. Rev. *34*, 344–363.

49. Duckworth, D.H., and Winkler, H.H. (1972). Metabolism of T4 bacteriophage ghost-infected cells. II. Do ghosts cause a generalized permeability change? J. Virol. *9*, 917–922.

50. Filali Maltouf, A.K., and Labedan, B. (1985). The energetics of the injection process of bacteriophage lambda DNA and the role of the ptsM pel-encoded protein. Biochem. Biophys. Res. Commun. *130*, 1093–1101.

51. Evilevitch, A., Lavelle, L., Knobler, C.M., Raspaud, E., and Gelbart, W.M. (2003). Osmotic pressure inhibition of DNA ejection from phage. Proc. Natl. Acad. Sci. USA *100*, 9292–9295.

52. Jeembaeva, M., Castelnovo, M., Larsson, F., and Evilevitch, A. (2008). Osmotic pressure: resisting or promoting DNA ejection from phage? J. Mol. Biol. *381*, 310–323.

53. Wu, D., Van Valen, D., Hu, Q., and Phillips, R. (2010). Ion-dependent dynamics of DNA ejections for bacteriophage λ. Biophys. J. *99*, 1101–1109.

54. Li, D., Liu, T., Zuo, X., Li, T., Qiu, X., and Evilevitch, A. (2015). Ionic switch controls the DNA state in phage λ. Nucleic Acids Res. *43*, 6348–6358.

55. Roessner, C.A., and Ihler, G.M. (1986). Formation of transmembrane channels in liposomes during injection of λ DNA. J. Biol. Chem. *261*, 386–390.

56. Kar, P., Tiruvadi-Krishnan, S., Männik, J., Männik, J., and Amir, A. (2023). Using conditional independence tests to elucidate causal links in cell cycle regulation in Escherichia coli. Proc. Natl. Acad. Sci. USA *120*, e2214796120.

57. Gabel, C.V., and Berg, H.C. (2003). The speed of the flagellar rotary motor of Escherichia coli varies linearly with protonmotive force. Proc. Natl. Acad. Sci. USA *100*, 8748–8751.

58. Kralj, J.M., Hochbaum, D.R., Douglass, A.D., and Cohen, A.E. (2011). Electrical spiking in Escherichia coli probed with a fluorescent voltage-indicating protein. Science *333*, 345–348.

59. Min, T.L., Mears, P.J., Golding, I., and Chemla, Y.R. (2012). Chemotactic adaptation kinetics of individual Escherichia coli cells. Proc. Natl. Acad. Sci. USA *109*, 9869–9874.

60. Min, T.L., Mears, P.J., Chubiz, L.M., Rao, C.V., Golding, I., and Chemla, Y.R. (2009). High-resolution, long-term characterization of bacterial motility using optical tweezers. Nat. Methods *6*, 831–835.

61. Keweloh, H.W., and Bakker, E.P. (1984). Increased permeability and subsequent resealing of the host cell membrane early after infection of Escherichia coli with bacteriophage T1. J. Bacteriol. *160*, 354–359.

62. Bonhivers, M., and Letellier, L. (1995). Calcium controls phage T5 infection at the level of the Escherichia coli cytoplasmic membrane. FEBS Lett. *374*, 169–173.

63. Sambrook, J., and Russell, D.; Cold Spring Harbor Laboratory (2001). Molecular Cloning: A Laboratory Manual, Third Edition, D.W. Russell, ed. (Cold Spring Harbor Laboratory).

64. Howard-Varona, C., Hargreaves, K.R., Abedon, S.T., and Sullivan, M.B. (2017). Lysogeny in nature: mechanisms, impact and ecology of temperate phages. ISME J. *11*, 1511–1520.

65. Luque, A., and Silveira, C.B. (2020). Quantification of lysogeny caused by phage coinfections in microbial communities from biophysical principles. mSystems *5*, e00353-20.

66. Geng, Y., Nguyen, T.V.P., Homaee, E., and Golding, I. (2023). Using population dynamics to count bacteriophages and their lysogens. Preprint at bioRxiv. https://doi.org/10.1101/2023.10.06.561271.

67. Lieb, M. (1953). The establishment of lysogenicity in Escherichia coli. J. Bacteriol. *65*, 642–651.

68. St-Pierre, F., and Endy, D. (2008). Determination of cell fate selection during phage lambda infection. Proc. Natl. Acad. Sci. USA *105*, 20705–20710.

69. Arkin, A., Ross, J., and McAdams, H.H. (1998). Stochastic kinetic analysis of developmental pathway bifurcation in phage λ-infected Escherichia coli cells. Genetics *149*, 1633–1648.

70. Alon, U. (2019). An Introduction to Systems Biology: Design Principles of Biological Circuits, Second Edition (CRC Press).

71. Boulanger, P., and Letellier, L. (1992). Ion channels are likely to be involved in the two steps of phage T5 DNA penetration into Escherichia coli cells. J. Biol. Chem. *267*, 3168–3172.

72. Benarroch, J.M., and Asally, M. (2020). The microbiologist's guide to membrane potential dynamics. Trends Microbiol. *28*, 304–314.

73. Galera-Laporta, L., Comerci, C.J., Garcia-Ojalvo, J., and Süel, G.M. (2021). IonoBiology: The functional dynamics of the intracellular metallome, with lessons from bacteria. Cell Syst. *12*, 497–508.

74. Chevallereau, A., Pons, B.J., van Houte, S., and Westra, E.R. (2022). Interactions between bacterial and phage communities in natural environments. Nat. Rev. Microbiol. *20*, 49–62.

75. Correa, A.M.S., Howard-Varona, C., Coy, S.R., Buchan, A., Sullivan, M.B., and Weitz, J.S. (2021). Revisiting the rules of life for viruses of microorganisms. Nat. Rev. Microbiol. *19*, 501–513.

76. Silveira, C.B., Luque, A., and Rohwer, F. (2021). The landscape of lysogeny across microbial community density, diversity and energetics. Environ. Microbiol. *23*, 4098–4111.

77. Koskella, B., Hernandez, C.A., and Wheatley, R.M. (2022). Understanding the impacts of bacteriophage viruses: from laboratory evolution to natural ecosystems. Annu. Rev. Virol. *9*, 57–78.

78. García, L.R., and Molineux, I.J. (1999). Translocation and specific cleavage of bacteriophage T7 DNA in vivo by EcoKI. Proc. Natl. Acad. Sci. USA *96*, 12430–12435.

79. Modell, J.W., Jiang, W., and Marraffini, L.A. (2017). CRISPR-Cas systems exploit viral DNA injection to establish and maintain adaptive immunity. Nature *544*, 101–104.

80. Borges, A.L., Zhang, J.Y., Rollins, M.F., Osuna, B.A., Wiedenheft, B., and Bondy-Denomy, J. (2018). Bacteriophage cooperation suppresses CRISPR-Cas3 and Cas9 immunity. Cell *174*, 917–925.e10.

81. Landsberger, M., Gandon, S., Meaden, S., Rollie, C., Chevallereau, A., Chabas, H., Buckling, A., Westra, E.R., and van Houte, S. (2018). Anti-CRISPR phages cooperate to overcome CRISPR-Cas immunity. Cell *174*, 908–916.e12.

82. Schindelin, J., Arganda-Carreras, I., Frise, E., Kaynig, V., Longair, M., Pietzsch, T., Preibisch, S., Rueden, C., Saalfeld, S., Schmid, B., et al. (2012). Fiji: an open-source platform for biological-image analysis. Nat. Methods *9*, 676–682.

83. Sanders, E.R. (2012). Aseptic laboratory techniques: plating methods. J. Vis. Exp. *63*, e3064.

84. Zeng, L., and Golding, I. (2011). Following cell-fate in E. coli after infection by phage lambda. J. Vis. Exp. *56*, e3363.

85. Zhang, K., Young, R., and Zeng, L. (2020). Bacteriophage P1 does not show spatial preference when infecting Escherichia coli. Virology *542*, 1–7.

86. Nielsen, H.J., Li, Y., Youngren, B., Hansen, F.G., and Austin, S. (2006). Progressive segregation of the Escherichia coli chromosome. Mol. Microbiol. *61*, 383–393.

87. Cohen, D., Melamed, S., Millman, A., Shulman, G., Oppenheimer-Shaanan, Y., Kacen, A., Doron, S., Amitai, G., and Sorek, R. (2019). Cyclic GMP–AMP signalling protects bacteria against viral infection. Nature *574*, 691–695.

88. Skinner, S.O., Sepúlveda, L.A., Xu, H., and Golding, I. (2013). Measuring mRNA copy number in individual Escherichia coli cells using single-molecule fluorescent in situ hybridization. Nat. Protoc. *8*, 1100–1113.

89. Yang, Y., Karin, O., Mayo, A., Song, X., Chen, P., Santos, A.L., Lindner, A.B., and Alon, U. (2023). Damage dynamics and the role of chance in the timing of E. coli cell death. Nat. Commun. *14*, 2209.

90. Brooks, K. (1965). Studies in the physiological genetics of some suppressor-sensitive mutants of bacteriophage λ. Virology *26*, 489–499.

91. Mears, P.J., Koirala, S., Rao, C.V., Golding, I., and Chemla, Y.R. (2014). Escherichia coli swimming is robust against variations in flagellar number. eLife *3*, e01916.

92. Leavitt, J.C., Gogokhia, L., Gilcrease, E.B., Bhardwaj, A., Cingolani, G., and Casjens, S.R. (2013). The tip of the tail needle affects the rate of DNA delivery by bacteriophage P22. PLoS One *8*, e70936.

93. Reichardt, L.F. (1975). Control of bacteriophage lambda repressor synthesis after phage infection: The role of the N, cII, cIII and cro products. J. Mol. Biol. *93*, 267–288.

94. Kobiler, O., Rokney, A., Friedman, N., Court, D.L., Stavans, J., and Oppenheim, A.B. (2005). Quantitative kinetic analysis of the bacteriophage λ genetic network. Proc. Natl. Acad. Sci. USA *102*, 4470–4475.

95. Papoulis, A. (1991). Probability, Random Variables, and Stochastic Processes (McGraw-Hill).

96. Arfken, G.B., Weber, H.J., and Harris, F.E. (2013). Mathematical Methods for Physicists: A Comprehensive Guide (Elsevier Science).

97. Grayson, P., Evilevitch, A., Inamdar, M.M., Purohit, P.K., Gelbart, W.M., Knobler, C.M., and Phillips, R. (2006). The effect of genome length on ejection forces in bacteriophage lambda. Virology *348*, 430–436.

98. Nurmemmedov, E., Castelnovo, M., Medina, E., Catalano, C.E., and Evilevitch, A. (2012). Challenging packaging limits and infectivity of phage λ. J. Mol. Biol. *415*, 263–273.

99. Gillespie, D.T. (2007). Stochastic simulation of chemical kinetics. Annu. Rev. Phys. Chem. *58*, 35–55.